BULLETIN OF THE POLISH ACADEMY OF SCIENCES
TECHNICAL SCIENCES, Vol. 73(1), 2025, Article number: e152216
DOI: 10.24425/bpasts.2024.152216

Mitigating sensor quality issues in UAV system identification through wavelet decomposition

Pedro JIMENEZ-SOLER* **and Piotr LICHOTA**

Institute of Aeronautics and Applied Mechanics, Warsaw University of Technology, 00-665 Warsaw, Poland

Abstract. Unmanned aerial vehicles (UAVs) require precise system identification for optimal performance and safety, yet sensor noise and signal distortion frequently compromise data quality. Recent studies have explored various approaches to mitigate these issues. However, this study introduces a novel method that utilizes wavelet transform techniques, distinctively enhancing UAV sensor signal processing. Unlike conventional methods that primarily focus on noise reduction, this approach employs multi-resolution wavelet decomposition to denoise and align signals effectively, crucial for accurate system identification. This systematic exploration of various wavelet bases and the application of the output error method for correlating signals provide a unique combination not extensively covered in current literature. The technique was validated using simulated sensor data at 50 Hz from a small UAV platform, the Multiplex®Fun Cub, specifically targeting longitudinal dynamics response. Results demonstrated substantial improvements in signal quality, with significantly enhanced correlation coefficients, showcasing the potential of our wavelet techniques to refine UAV system analysis. This paper presents a comprehensive framework for applying wavelet-based techniques in UAV system identification, significantly advancing the robustness and reliability of identification processes and distinguishing our work from existing methods by its integration of wavelet decomposition and advanced system identification techniques.

Keywords: unmanned aerial vehicles (UAVs); wavelet transform; time synchronization; system identification; noise reduction; aerodynamics; flight mechanics.

1. INTRODUCTION

System identification for unmanned aerial vehicles (UAVs) critically relies on the accurate and reliable acquisition of data from well-calibrated sensors [1]. However, sensor fidelity often diminishes in low-speed, low-cost fixed-wing UAVs, introducing substantial noise and inaccuracies into flight test data [2]. Such distortions can severely impair the effectiveness of system identification processes essential for validating aerodynamic models, optimizing controllers, and enhancing flight safety and efficiency [3–5].

Recent advancements in signal processing have spotlighted wavelet transforms as a potent tool for refining system identification by adeptly managing signals corrupted by noise [6, 7]. This technique allows for the decomposition of a signal into its constituent frequency components, facilitating the isolation and rectification of distortions typical in data from low-quality sensors [6]. Although wavelet transforms have been employed across various aerospace applications, their integration into UAV system identification remains underexplored, particularly in the context of dynamic and uncertain environmental conditions [1, 8, 9].

This study introduces a novel methodology that leverages wavelet decomposition combined with correlation coefficients to enhance signal integrity from UAV sensors [1, 10–13]. Unlike existing methods, which often do not address the compounded challenges of noise and computational limitations in UAV applications [14–16], this approach utilizes aerodynamic derivatives from simulations as a priori values to significantly refine the accuracy of system identification [17–20]. This paper delineates how this method not only mitigates the impact of sensor noise but also aligns with contemporary computational techniques to improve predictions of UAV behaviour and the reliability of derived control systems.

Distinctly, this research extends the current understanding by demonstrating how a dual-domain approach—employing both time and frequency characteristics of wavelet-transformed signals – can robustly enhance model accuracy and resilience against noise. These findings are substantiated by improved correlation coefficients post-alignment, showcasing the method capability to offer precise and reliable system identification under real-world operational conditions. This advancement marks a significant step forward in the application of wavelet techniques in aerospace, particularly in optimizing system identification processes for UAVs subjected to low-quality sensor data [11, 21–23].

The structure of this paper is as follows. Section 1 introduces the necessity of precise system identification and how wavelet decomposition aids in mitigating sensor noise. Section 2 delves into the dynamic modelling of UAVs, detailing the development and significance of the longitudinal dynamic model using the Multiplex FunCub®R/C airplane. Noise implementation and its effect on sensor data quality is explored in Section 3. The subsequent Sections 4 and 5 discuss wavelet analysis and the applica-

*e-mail: pedro.jimenez_soler.dokt@pw.edu.pl

Manuscript submitted 2024-08-09, revised 2024-09-17, initially accepted for publication 2024-10-09, published in January 2025.

tion of the output error method for system identification under different noise conditions. Section 6 presents a detailed correlation analysis, comparing the effectiveness of wavelet-based signal reconstruction in enhancing the accuracy of system identification from noisy and noise-free UAV sensor data. Finally, the paper concludes by summarizing the findings and implications for future research in Section 7, providing a pathway for ongoing advancements in UAV system analysis.

2. UNMANNED AIRCRAFT VEHICLE DYNAMIC MODEL

The precision of unmanned aerial vehicle (UAV) operations centers on the reliability and accuracy of its system identification, which is deeply influenced by the fidelity of its dynamic modelling [24]. This study developed a dynamic model focusing particularly on its longitudinal dynamics [19]. This model is the base for subsequent analyses involving wavelet-based signal processing and system identification techniques under various noise conditions.

The model parameters influencing longitudinal flight dynamics are listed in Table 1. Initial conditions for the simulation, including airspeed, angle of attack, pitch angle, and pitch rate, were set based on typical flight conditions obtained in flight tests. Then, aerodynamic forces and moments acting on the aircraft were computed at each step of the integration process, based on the current states [18]. These computations feed into the state equations and variables shown in Section 2.2. The output from the solver provided detailed time histories of these states, which were crucial for the subsequent noise addition simulating real-world low-cost sensors.

Table 1
Aircraft parameters

Parameter	Symbol	Value	Unit
Moment of inertia around pitch axis	Iyy	0.09504	kg·m^2
Mean aerodynamic chord	c	0.226	metres
Aircraft mass	m	1.96	kg
Wing area	S	0.313	m^2
Cruise velocity	V_0	21	m/s

2.1. Multiplex FunCub R/C airplane longitudinal dynamic model

The Multiplex FunCub®R/C airplane [25] was chosen for this study due to its versatility and adaptability in carrying various sensors and payloads, ideal for experimental UAV system identification, as shown in Fig. 1 [26]. As a low-speed, lightweight model, it accurately represents typical UAVs used in research and practical applications, allowing for detailed analysis and testing of wavelet transform techniques under controlled yet realistic conditions. This platform facilitates the simulation of noise effects on sensor data, which is crucial for developing and validating advanced signal processing methods.

Fig. 1. Multiplex FunCub® airplane

2.2. Longitudinal state equations

The longitudinal dynamics are crucial for understanding and predicting its behaviour under various flight conditions. These dynamics can be effectively captured through a set of state equations that describe the behavior of state variables as the aircraft's velocity V, angle of attack α, pitch angle θ, and pitch rate q [18, 19, 24]. These state equations are derived from the fundamental principles of flight dynamics and are influenced by aerodynamic forces and aircraft control inputs, such as elevator deflection and engine thrust [18]. In this model, lateral-directional effects are considered decoupled, though similar methodologies could be applied to model lateral-directional motion [18].

The longitudinal motion is governed by the following state equations in continuous time, which integrate aerodynamic coefficients, control deflections, and external forces as shown in equations (1)–(4):

$$\dot{V} = -\frac{\bar{q}S}{m}C_D + g\sin(\alpha-\theta) + \frac{F_e}{m}\cos(\alpha+\sigma_T), \tag{1}$$

$$\dot{\alpha} = -\frac{\bar{q}S}{mV}C_L + q + \frac{g}{V}\cos(\alpha-\theta) - \frac{F_e}{mV}\sin(\alpha+\sigma_T), \tag{2}$$

$$\dot{\theta} = q, \tag{3}$$

$$\dot{q} = \frac{\bar{q}S\bar{c}}{I_y}C_m + \frac{F_e}{I_y}(l_{tx}\sin\sigma_T + l_{tz}\cos\sigma_T), \tag{4}$$

where the drag equation (5), lift equation (6), and pitching moment coefficients equation (7) are modelled as:

$$C_D = C_{D0} + C_{DV}\frac{V}{V_0} + C_{D\alpha}\alpha, \tag{5}$$

$$C_L = C_{L0} + C_{LV}\frac{V}{V_0} + C_{L\alpha}\alpha, \tag{6}$$

$$C_m = C_{m0} + C_{mV}\frac{V}{V_0} + C_{m\alpha}\alpha + C_{mq}\frac{q\bar{c}}{2V_0} + C_{m\delta_e}\delta_e. \tag{7}$$

The symbols in equations (1)–(7) represent parameters of aircraft longitudinal dynamics. $\dot{V}$, $\dot{\alpha}$, $\dot{q}$, and $\dot{\theta}$ denote the rates of velocity change, angle of attack, pitch rate, and pitch angle, respectively, $\bar{q}$ denotes dynamic pressure, while S, m, and I_y are the wing area, aircraft mass, and moment of inertia about the pitch axis. Aerodynamic coefficients C_D, C_L and C_m depend on velocity V, angle of attack α, and pitch rate q, modified by respective coefficients that account for conditions like baseline velocity V_0 and elevator deflection δ_e. Additional parameters include g for gravitational acceleration, F_e for engine thrust, and σ_T, l_{tx}, and l_{tz} for thrust line angles and distances relative to

the centre of gravity. These elements collectively model aircraft response to control inputs and environmental factors.

Initial aerodynamic coefficients and parameters were determined using XFLR5, an analysis tool for airfoils, wings, and planes operating at low Reynolds numbers [27]. XFLR5 uses panel methods and vortex lattice models to compute coefficients and performance metrics, providing essential preliminary insights for aerodynamic modelling [28].

The values obtained from XFLR5 were treated as a priori estimates, serving as the initial set of parameters for system identification [29]. These a priori values are critical as they establish a baseline from which the system behaviour can be studied. Coefficients are listed in Table 2.

Table 2
Aerodynamic coefficients a priori values from XFLR5

Coefficient description		Value
Lift coefficient at zero angle of attack	CL_0	0.1518
Lift coefficient due to angle of attack	CL_α	4.2305
Lift coefficient due to velocity	CL_v	–0.0025
Drag coefficient at zero angle of attack	CD_0	0.0177
Drag coefficient due to angle of attack	CD_α	0.1223
Drag coefficient due to velocity	CD_v	0.0136
Pitching moment coefficient at zero angle of attack	Cm_0	0.0446
Pitching moment coefficient due to angle of attack	Cm_α	–1.6173
Pitching moment coefficient due to pitch rate	Cm_q	–8.0193
Pitching moment coefficient due to elevator deflection	$Cm_{\delta e}$	–1.4830
Pitching moment coefficient due to velocity	Cm_v	–0.0092

2.3. Multistep input signal design

The design of input signals for dynamic system identification must strategically excite all modes of the system to ensure that all dynamic behaviours are adequately observed [30]. The analysis emphasizes the importance of designing multistep elevator input signals for longitudinal aircraft motion [31, 32]. It highlights that the optimal frequency range should extend both below and above the natural frequency of the short-period mode due to inherent uncertainties in eigenfrequencies, which also vary with flight conditions. Consequently, it is crucial to excite frequencies surrounding the eigenfrequency. Such signals can be crafted using a series of equidistant pulse inputs, forming a signal of arbitrary shape and amplitude levels to match the power spectrum requirements [18].

Therefore, the development of multistep input signals involves a sequential approach: initially determining the spectrum of frequencies essential for precise parameter estimation, followed by the crafting of appropriately structured multistep inputs to span these identified frequencies [33, 34].

The assessment of the necessary frequency range for precise parameter estimation involves synthesizing the contributions of each parameter featured in the force and moment equations. This process is facilitated by using Bode diagrams, which assist in identifying the required frequencies in the input signal for the accurate extraction of specific aerodynamic derivatives. The methodology, initially developed by Marchand [35], is demonstrated using a linearized model for longitudinal motion, which explores the identifiability of aircraft derivatives from flight tests or simulations as data shown in Table 2 from XFLR5 software. Thus, for each expression presented in equation (8), the magnitudes of the frequency responses from the terms are graphically represented as a function of the frequency of the input signal

$$\begin{bmatrix} \dot{V} \\ \dot{\alpha} \\ \dot{q} \\ \dot{\theta} \end{bmatrix} = \begin{bmatrix} X_u & X_\alpha & X_q & -g \\ Z_u/U_0 & Z_\alpha/U_0 & 1 & 0 \\ M_u & M_\alpha & M_q & 0 \\ 0 & 0 & 1 & 0 \end{bmatrix} \begin{bmatrix} V \\ \alpha \\ q \\ \theta \end{bmatrix} + \begin{bmatrix} X_{\delta_e} \\ Z_{\delta_e} \\ M_{\delta_e} \\ 0 \end{bmatrix} \delta_e \,. \tag{8}$$

The frequency range to identify aerodynamic coefficients is between 0.1 rad/s to 10 rad/s for short periods and phugoid modes. As a rule of thumb, a derivative is considered identifiable when its term has a magnitude of at least 10% of the largest term magnitude [18], for this case, a frequency of $f_c = 0.468$ rad/s is selected. Hence, the time interval Δt for the input is selected to position the natural frequency of the targeted mode either centrally or within the upper third of the input signal spectrum [18].

Based on these observations, a Multistep 3-2-1-1 input signal is chosen as the most affordable [36]. The estimated Δt for the 3-2-1-1 input configuration can be determined as follows in equation (9):

$$\Delta t_{3\text{-}2\text{-}1\text{-}1} \approx \frac{0.3}{f_c} = 0.641 \text{ s}. \tag{9}$$

As a result, the elevator deflection function of 60s time length, 0.1deg of amplitude, and $\Delta t = 0.641$ s is selected for the 3-2-1-1 excitation. Input deflection is designed to excite aircraft longitudinal dynamics, capturing both the short-period and phugoid response across a spectrum of frequencies previously described as shown in Fig. 2.

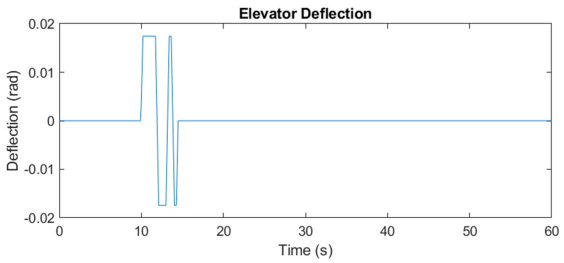

Fig. 2. Multistep 3-2-1-1 elevator deflection signal

3. NOISE IMPLEMENTATION

In this section, the implementation of noise to UAV sensor data is described. To replicate these conditions within a controlled environment, noise is artificially introduced to the pre-recorded signal data, further incorporating a realistic offset to mimic sensor drift. The procedure begins with loading the simulation data, which contains multiple channels representing different flight parameters, as shown in Table 3.

Table 3
Channel data definition

No.	Symbol	Unit	Description
1	T	S	Time
2	DELV	RAD	Elevator deflection
3	PDYN	PA	Dynamic pressure
4	THRUST	N	Thrust
5	TASCG	M/S	True airspeed at CG
6	ALFCG	RAD	Angle of attack at CG
7	THE	RAD	Pitch attitude
8	Q	RAD/S	Pitch rate
9	QDOT	RAD/S^2	Pitch acceleration
10	AXCG	M/S^2	Longitudinal acceleration at CG
11	AZCG	M/S^2	Lateral acceleration at CG

Each channel shown in Table 3, except for the time column, is then subjected to a calculated noise addition process, where Gaussian noise is specifically tailored to achieve a desired signal-to-noise ratio (SNR) of 10 dB. This level was chosen to simulate a moderate yet significant noise level that challenges the robustness of the system identification algorithms [37]. To introduce the noise, the standard deviation of the noise is derived based on the desired SNR of 10 dB and the standard deviation of the original signal within each channel. Power spectrum density (PSD) analysis was also employed to further understand the energy distribution of the signal across different frequencies, as shown in Fig. 3.

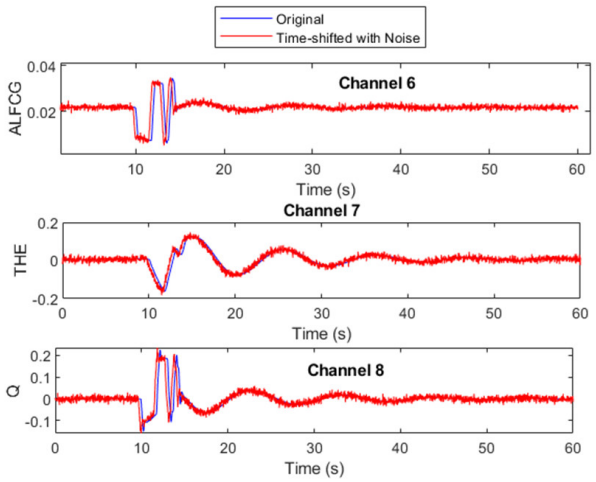

Fig. 3. Multiplex FunCub noisy responses

Additionally, a time shift of 0.3 seconds was applied to the entire dataset to simulate a common real-world issue of sensor lag or misalignment. This time shift is computed based on the sampling rate derived from the time intervals of the dataset, ensuring the shift is accurately represented across all data points. This is essential for testing the adaptive capabilities of the system identification techniques under study [38].

Finally, the altered dataset "*noisy*" is the further input for the following sections, preserving the integrity of the original data while providing a realistic test scenario.

4. WAVELET ANALYSIS

Wavelet decomposition involves breaking down a time-series signal into its constituent scales or frequencies using wavelets. This technique is advantageous for handling nonstationary signals commonly encountered in UAV operations, where sensor readings often fluctuate due to varying flight dynamics, environmental conditions, and sensor noise. In this study, the *Haar* wavelet was selected for its simplicity and effectiveness in capturing signal discontinuities and shifts [39]. The decomposition process was applied to both simulated clean and noisy sensor data from the UAV, aiming to assess the method robustness against noise. The discrete wavelet transform (DWT) provided a multi-resolution analysis, allowing the isolation and examination of signal components across different frequency bands.

Signals were decomposed into a set of wavelet coefficients at specified decomposition levels [40]. The choice of decomposition level was determined based on the frequency content necessary to capture the dynamics of the UAV.

4.1. Wavelet decomposition

The wavelet transform facilitates the decomposition of a primary signal into its constituent elements, each reflecting specific frequency characteristics detectable at distinct times [1, 11]. This decomposition is achieved through the application of a series of functions known as wavelets, which are scaled and translated across the signal. The mathematical representation of a wavelet function is given by equation (10):

$$\psi_{a,b}(t) = \frac{1}{\sqrt{a}}\psi\left(\frac{t-b}{a}\right), \tag{10}$$

where ψ represents the wavelet function, a is the scale parameter affecting the frequency, and b is the time offset parameter, determining the wavelet's position along the signal. For practical applications, the discrete wavelet transform (DWT) is used. The DWT employs the Mallat algorithm, also known as the pyramid scheme, which simplifies the signal into layers of approximations and details [41]. This method ensures that each level of decomposition maintains a consistent number of data points, essential for accurately reconstructing the original signal. The coefficients for approximation and detail in the context of multiple flight parameters can be mathematically expressed using the following relationships expressed in equations (11) and (12):

$$A_l^{i,j} = \sum_k h_\psi[k-2l]A_k^{i,j-1}, \tag{11}$$

$$D_l^{i,j} = \sum_k g_\psi[k-2l]D_k^{i,j-1}, \tag{12}$$

where i denotes the flight parameter index, j the level of decomposition, and k represents the discrete frequency. The functions (h_ψ) and (g_ψ) are the respective high-pass and low-pass filters, which are applied after a delay of $(2l)$. Then, the Haar wavelet is defined by the function in equation (13):

$$\Psi(t) = \begin{cases} 1 & 0 \le t < 0.5, \\ -1 & 0.5 \le t < 1, \\ 0 & t \notin [0\ 1). \end{cases} \tag{13}$$

While other types of wavelets like Daubechies or Meyer could also be used, the Haar wavelet was preferred due to its simplicity and effectiveness, which aligns with the findings presented at the end of this section. For validating the outcomes from wavelet decomposition, the signal reconstruction formula incorporated into the system identification process is shown in equation (14):

$$y_i = \sum_l h_\Psi[k-2l]A_k^{i,j} + \sum_j \sum_l g_\Psi[k-2l]D_k^{i,j}. \tag{14}$$

For this study, the simulation model was configured with a time step of 0.02 seconds to align with the standard 50 Hz sampling rate commonly employed in aircraft system identification [7,18]. The decomposition process was conducted up to level 11 to encompass a wide dynamic spectrum, suitable for the expected aircraft modes occurring below 9.5 rad/s. The specific frequency ranges are captured at various decomposition levels, focusing on the finer frequencies between 0.19531 Hz and 3.125 Hz, which are critical for accurately characterizing aircraft dynamics from the noise-free signal. As a matter of fact, decomposition level 4 was the lowest used for parameter estimation, with level 7 providing the highest detail and best correlation results. Parameter estimation focused on 60 seconds of flight data at level 7, balancing detail and computational efficiency to capture aircraft dynamics within this timeframe effectively.

4.2. Original and noisy reconstruction

Wavelet decomposition was applied to both original and noisy datasets using MATLAB software working with wavelet analysis functions, which facilitated the processing of UAV sensor data. The signals were specifically reconstructed at the seventh level of decomposition, as shown in Fig. 4. This figure displays the original and reconstructed signals for channel 7, highlighting the pitch response derived from both noise-free and noisy data.

For each channel, wavelet decomposition was followed by the reconstruction of both the approximation and detail coefficients at the seventh level. The resultant reconstructed signals for both original and noisy datasets are then stored in ASCII format for further system identification.

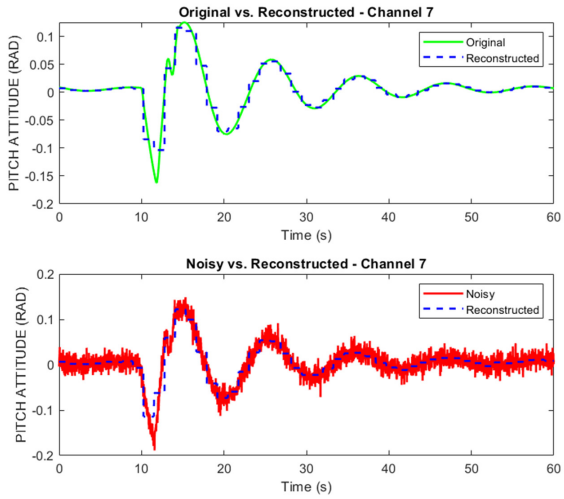

Fig. 4. Original and noisy signals reconstruction

4.3. Reconstructed cases – wavelet decomposition

In this section, a detailed correlation analysis between reconstructed noisy signals and their corresponding noise-free counterparts was conducted to evaluate the efficacy of the wavelet-based signal reconstruction technique.

The primary objective was to determine the optimal time shifts and the corresponding maximum correlation coefficients for each channel. This involved adjusting the noisy data within a shift range of −20 to +20 samples and calculating the correlation coefficient against the original, noise-free data for each possible shift [2].

This iterative process allowed for identifying the shift value that maximized the correlation coefficient for each channel, thus potentially correcting any misalignments caused by noise or other factors.

Figure 5 illustrates the correlation analysis between noise-free reconstructed signals and their corresponding noisy, shifted reconstructions across several channels of flight data.

A notable alignment between the two signal types, with correlation coefficients ranging from 0.91 to 0.98. These high correlation values indicate that the wavelet-based signal reconstruction, followed by optimal shifting, effectively minimizes the discrepancies caused by noise.

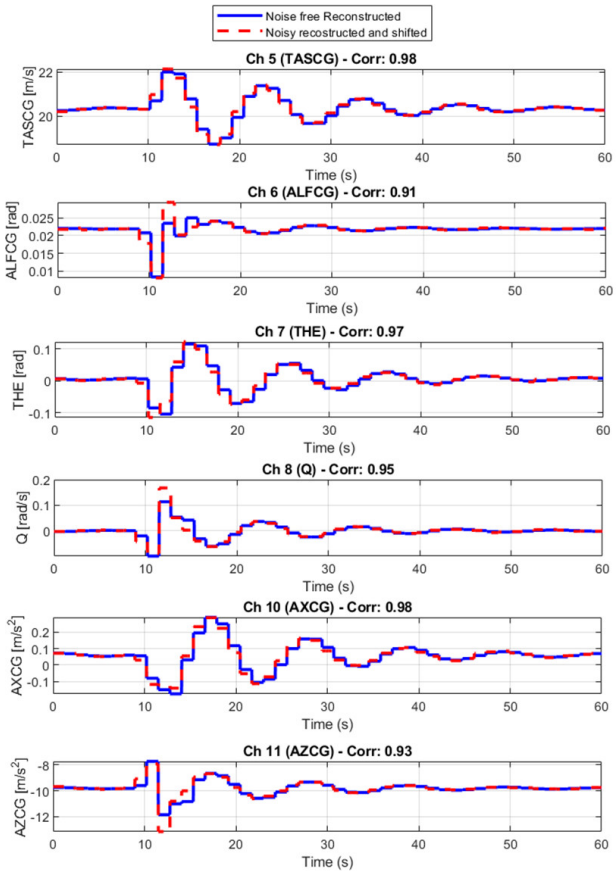

Fig. 5. Noise-free, reconstructed and shifted correlations

5. OUTPUT ERROR METHOD – SYSTEM IDENTIFICATION

The previous section demonstrated how wavelet decomposition can mitigate noise from low-cost sensors, enhancing model robustness and accuracy with system identification methods that assess noise-free, noisy, and wavelet-reconstructed data. This section introduces the output error method (OEM), a powerful system identification technique used to derive dynamic characteristics from measured data [18].

The focus is on applying OEM to UAV system identification, specifically for determining aerodynamic derivatives and aircraft state behaviours. OEM iteratively refines model parameters to fit the data optimally, proving effective in handling noisy and nonlinear conditions [15], crucial for managing the intricate dynamics of UAVs [4]. In this study, the OEM is applied under three distinct conditions: using noise-free data, using data corrupted with simulated sensor noise, and using data reconstructed via wavelet decomposition techniques. The goal is to evaluate the performance of the system identification process under varying levels of data quality, highlighting the potential benefits of wavelet preprocessing in enhancing the accuracy of the identified system models. The method iteratively adjusts the model parameters to achieve the best fit with the experimental data. The primary equation for the output error $e(t)$ is shown in equation (15):

$$e(t) = y(t) - \hat{y}(t,\theta), \tag{15}$$

where $y(t)$ represents the measured output, $\hat{y}(t,\theta)$ is the predicted output from the model dependent on parameters θ, and t indicates the time. The core objective in OEM is to minimize the sum of the squared errors, formulated in equation (16):

$$J(\theta) = \sum_{t=1}^{T} [y(t) - \hat{y}(t,\theta)]^2 . \tag{16}$$

This sets up an optimization problem to find the parameter set θ^*, and it results in the minimum cost as shown in equation (17):

$$\theta^* = \arg\min_{\theta} J(\theta). \tag{17}$$

Then, the maximum likelihood estimation (MLE) is employed to enhance the parameter estimation by assuming that the errors $e(t)$ are probabilistically modelled, as normally distributed with zero mean and constant variance. This assumption aligns with the principle of maximizing the likelihood that the observed data could be produced by the model parameters. The process involved an iterative optimization loop where UAV system outputs were simulated, and parameters adjusted to minimize the discrepancy between model predictions and observed data.

5.1. Noise-free and noisy OEM cases

The noise-free dataset was initially employed for system identification to establish a baseline of accuracy and evaluate the method efficiency, achieving a maximum relative standard deviation (RSD) of 0.76. Convergence was reached within seven iterations, affirming the method precision. Subsequently, OEM was applied to the noisy dataset, resulting in a higher maximum relative standard deviation of 16.09 after five iterations, as depicted in Fig. 6.

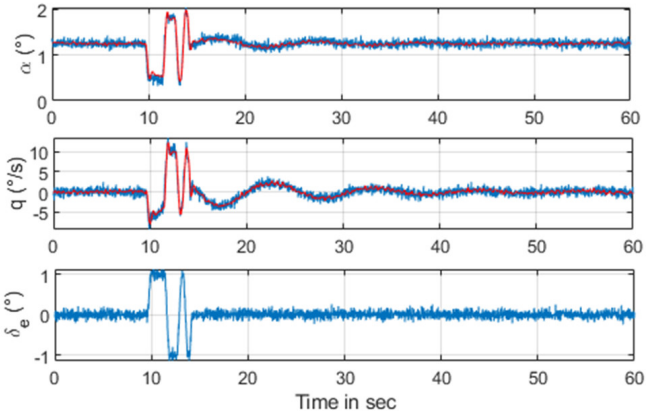

Fig. 6. Measured and estimated data – noise case

5.2. Reconstructed cases – wavelet decomposition

OEM was also applied to data reconstructed through wavelet decomposition techniques, studying its effectiveness under varying levels of noise reduction and signal restoration. This phase evaluated preprocessing data using wavelet transform as input data to the system identification script, resulting in a higher maximum relative standard deviation of 6.09 after 11 iterations, demonstrating the method robustness under wavelet reconstruction, as shown in Fig. 7. Table 4 presents the relative standard deviation (RSD) of the parameter Cmq estimation, illustrating the high accuracy of system identification when employing the reconstructed signal compared to estimations derived from a priori values in a noisy environment.

Table 4

Comparison of estimation of pitching moment coefficient due to pitch rate – Cmq [1/rad/s]

	A priori XFLR5	Clear simulated	Noisy simulated	Wavelet reconstructed
Estimated value	–8.01	–7.06	–1.61	–7.12
RSD	–	0.76	16.09	0.86

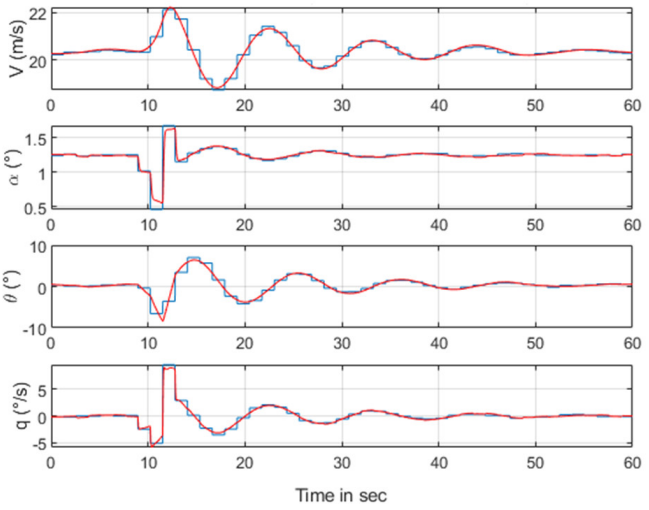

Fig. 7. Measured and estimated data – wavelet reconstructed

6. CORRELATION ANALYSIS

This section contrasts system identification outcomes for datasets with and without noise, both before and after applying wavelet reconstruction. Each plot features two lines: a blue line for the system identification from clean data and a red dashed line for the noisy data. Correlation coefficients, noted in the plot legends, quantify the alignment between these two results. Figure 8 displays correlations between 0.92 and 0.96, indicating some discrepancies possibly due to signal drift and shifting, leading to higher relative errors as previously noted. In contrast, Fig. 8 exhibits improved correlations, particularly for the pitch rate parameter at 0.98, suggesting enhanced accuracy in system identification after noise removal via wavelet reconstruction. The effectiveness of this approach is further validated by the lower relative errors shown in Table 5, which presents estimation errors post-reconstruction.

7. CONCLUSIONS

This study improves UAV system identification by using wavelet decomposition to enhance the handling of noise from low-cost sensors. Unlike traditional methods primarily focusing on noise filtering, this research introduces wavelet-based signal reconstruction which provides a sophisticated means of restoring data integrity. The methodology employed here shows marked improvements in correlation coefficients and reduced error margins, setting it apart from other methods cited in recent studies such as [1, 10–13]. This approach uniquely combines the robustness of wavelet transformations with practical system identification techniques, offering a significant enhancement in model accuracy and reliability under noisy conditions.

The primary advantage of the proposed method lies in its ability to effectively isolate and correct distorted signal components, which are typically challenging to manage with low-cost UAV

Table 5
Relative errors in aerodynamic parameters

Parameter	CD0	CDV	CDAL	CL0	CLV	CLAL	CM0	CMAL	CMQ	CMV	CMDE
Relative error	0.03%	5.13%	0.57%	0.37%	–4.52%	–0.10%	0.71%	–0.78%	4.64%	3.11%	–0.80%

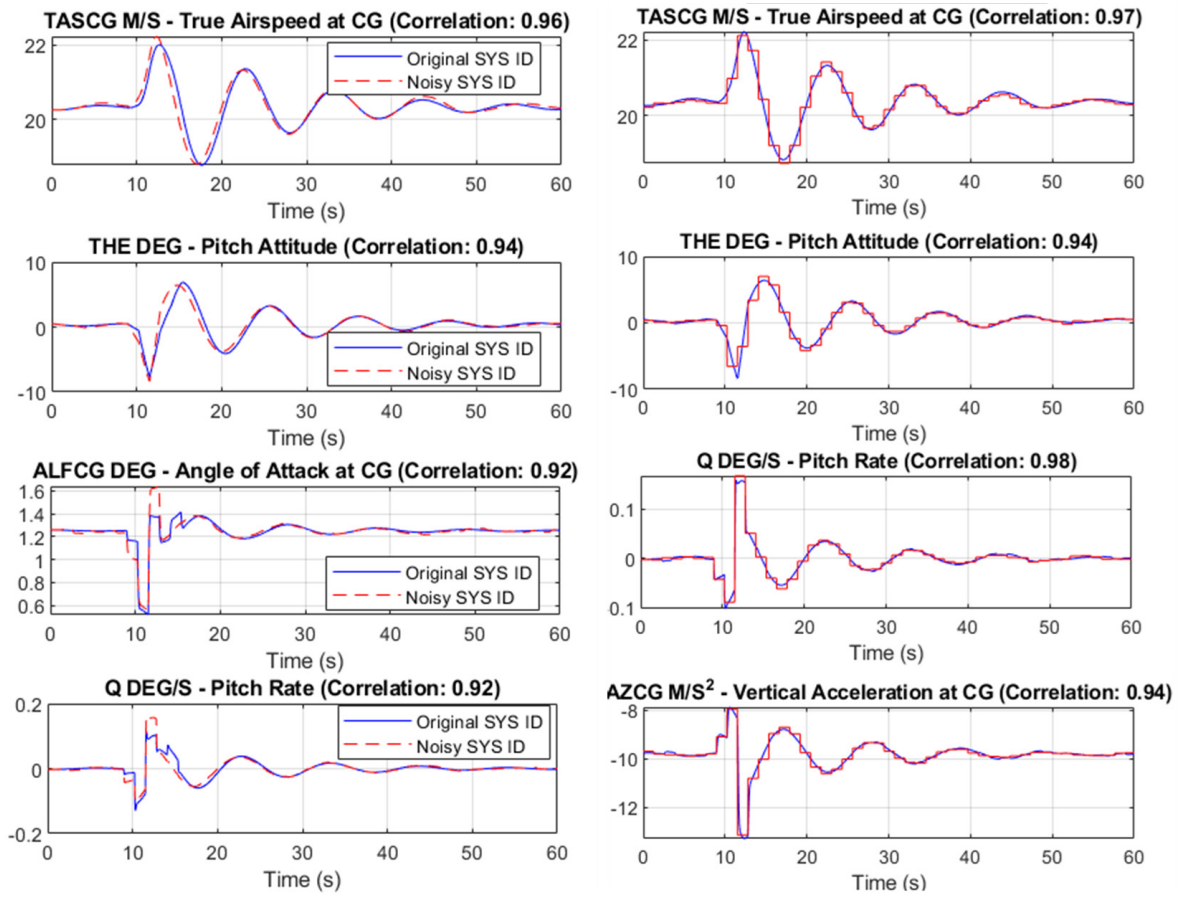

(a) (b)

Fig. 8. Comparison between identified signals (noise-free and noisy (a) and noisy and reconstructed (b)

sensors. This leads to more accurate system identification, even in the presence of significant environmental and sensor noise. However, one limitation is the computational complexity associated with wavelet transformations, which may extend processing times or require more powerful computing resources [42]. Future improvements might focus on optimizing the algorithm to reduce computational demands or exploring more efficient wavelet bases that balance performance and computational overhead [41].

Looking forward, the methodology presented in this paper lays a solid foundation for further research into adaptive noise management techniques in UAV system identification. Future studies could explore the integration of real-time adaptive filtering techniques to enhance the responsiveness of the system identification process to dynamic changes. Finally, further analysis will validate the proposed method using real flight-test data, which can be sourced from new experimental studies [4, 18].

REFERENCES

[1] P. Lichota, "Wavelet Transform-Based Aircraft System Identification," *J. Guid. Control Dyn.*, vol. 46, no. 2, pp. 350–361, Feb. 2023, doi: 10.2514/1.G006654.

[2] P. Kapler, "An application of continuous wavelet transform and wavelet coherence for residential power consumer load profiles analysis," *Bull. Pol. Acad. Sci. Tech. Sci.*, vol. 69, no. 1, p. e136216, 2021, doi: 10.24425/bpasts.2020.136216.

[3] S.K. Fatima, M. Abbas, I. Mir, S. Mir, and F. Gul, "A Perspective Analysis on Effects of Varying Inputs on UAV Model Estimation," *J. Intell. Robot. Syst.*, vol. 108, no. 4, p. 71, Jul. 2023, doi: 10.1007/s10846-023-01889-0.

[4] B.M. Simmons, J.L. Gresham, and C.A. Woolsey, "Flight-Test System Identification Techniques and Applications for Small, Low-Cost, Fixed-Wing Aircraft," *J. Aircr.*, vol. 60, no. 5, pp. 1503–1521, Sep. 2023, doi: 10.2514/1.C037260.

[5] S.K. Fatima, S.M. Abbas, I. Mir, F. Gul, and A. Forestiero, "Flight Dynamics Modeling with Multi-Model Estimation Techniques: A Consolidated Framework," *J. Electr. Eng. Technol.*, vol. 18, no. 3, pp. 2371–2381, May 2023, doi: 10.1007/s42835-023-01376-4.

[6] D. Zhang, "Wavelet Transform," in *Fundamentals of Image Data Mining: Analysis, Features, Classification and Retrieval*, D. Zhang, Ed., Cham: Springer International Publishing, 2019, pp. 35–44, doi: 10.1007/978-3-030-17989-2_3.

[7] T. Guo, T. Zhang, E. Lim, M. López-Benítez, F. Ma, and L. Yu, "A Review of Wavelet Analysis and Its Applications: Challenges and Opportunities," *IEEE Access*, vol. 10, pp. 58869–58903, 2022, doi: 10.1109/ACCESS.2022.3179517.

[8] F.C. Sanders, M. Tischler, T. Berger, M.G. Berrios, and A. Gong, "System Identification and Multi-Objective Longitudinal Control Law Design for a Small Fixed-Wing UAV," in *2018 AIAA Atmospheric Flight Mechanics Conference*, Kissimmee, Florida, Jan. 2018, doi: 10.2514/6.2018-0296.

[9] M.A. Cunningham and J.E. Hubbard, "Open-Loop Linear Model Identification of aMultirotor Vehicle with Active Feedback Control," *J. Aircr.*, vol. 57, no. 6, pp. 1044–1061, Nov. 2020, doi: 10.2514/1.C035834.

[10] O. Medaiyese, M. Ezuma, A.P. Lauf, and I. Guvenc, "Wavelet transform analytics for RF-based UAV detection and identification system using machine learning," *Pervasive Mob. Comput.*, vol. 82, p. 101569, Jun. 2022, doi: 10.1016/j.pmcj.2022.101569.

[11] M. Naruoka, T. Hino, and T. Tsuchiya, "Application of Wavelet Transform to System Identification of Small UAVs Flight Characteristic," in *AIAA Infotech@Aerospace 2010*, 2010, doi: 10.2514/6.2010-3536.

[12] S. Tong, Z. Shi, T. Yun, and Y. Dong, "Longitudinal flight dynamics modeling and a flight stability analysis of a monocopter," *AIP Adv.*, vol. 12, no. 11, p. 115322, Nov. 2022, doi: 10.1063/5.0130626.

[13] S. Zhou, Z. He, X. Chen, and W. Chang, "An Anomaly Detection Method for UAV Based on Wavelet Decomposition and Stacked Denoising Autoencoder," *Aerospace*, vol. 11, no. 5, p. 5, May 2024, doi: 10.3390/aerospace11050393.

[14] L.E. Hale, M. Patil, and C.J. Roy, "Aerodynamic Parameter Identification and Uncertainty Quantification for Small Unmanned Aircraft," *J. Guid. Control Dyn.*, vol. 40, no. 3, pp. 680–691, Mar. 2017, doi: 10.2514/1.G000582.

[15] E. Balestrieri, P. Daponte, L. De Vito, F. Picariello, and I. Tudosa, "Sensors and Measurements for UAV Safety: An Overview," *Sensors*, vol. 21, no. 24, p. 24, Jan. 2021, doi: 10.3390/s21248253.

[16] J. Peng, P. Zhang, L. Zheng and J. Tan, "UAV Positioning Based on Multi-Sensor Fusion," *IEEE Access*, vol. 8, pp. 34455–34467, 2020, doi: 10.1109/ACCESS.2020.2974285.

[17] L. Kivistik, M. Mehrparvar, M. Eerme, and J. Majak, "Dynamics of flight of the fragments with higher order Haar wavelet method," *P. Est. Acad. Sci.*, vol. 73, no. 2, p. 108, 2024, doi: 10.3176/proc.2024.2.02.

[18] R.V. Jategaonkar, *Flight Vehicle System Identification: A Time-Domain Methodology, Second Edition*. Reston, VA: American Institute of Aeronautics and Astronautics, Inc., 2015, doi: 10.2514/4.102790.

[19] B.N. Pamadi, *Performance, Stability, Dynamics, and Control of Airplanes, Third Edition*. Reston, VA: American Institute of Aeronautics and Astronautics, Inc., 2015, doi: 10.2514/4.102745.

[20] P. Jimenez, P. Lichota, D. Agudelo, and K. Rogowski, "Experimental Validation of Total Energy Control System for UAVs," *Energies*, vol. 13, no. 1, p. 14, Dec. 2019, doi: 10.3390/en13010014.

[21] I.-R. Edu, F.-C. Adochiei, P. Negrea, C. Rotaru, and T.L. Grigorie, "New Tuning Method of the Wavelet Function for Inertial Sensors Signals Denoising," in *CSCC14. Org and EUROPMENT Conferences*, 2014, pp. 16–18. [Online]. Available: https://inase.org/library/2014/santorini/bypaper/MATH/MATH-22.pdf (Accessed: Aug. 04, 2024).

[22] P. Lichota, "Unstable tilt-rotor maximum likelihood wavelet-based identification from flight test data," *Aircr. Eng. Aerosp. Technol.*, vol. 95, no. 8, pp. 1275–1285, Jul. 2023, doi: 10.1108/Aircr.Eng.Aerosp.Technol.-01-2023-0013.

[23] H. Mwenegoha, T. Moore, J. Pinchin, and M. Jabbal, "Model-Based Autonomous Navigation with Moment of Inertia Estimation for Unmanned Aerial Vehicles," *Sensors*, vol. 19, no. 11, p. 11, Jan. 2019, doi: 10.3390/s19112467.

[24] M.V. Cook, *Flight Dynamics Principles: A Linear Systems Approach to Aircraft Stability and Control*. Butterworth-Heinemann, 2012.

[25] Multiplex, "Multiplex Fun cub Manual." Hitecrcd, 2024. [Online]. Available: https://hitecrcd.com/files/FunCubManual.pdf (Accessed: Jan. 08, 2024).

[26] "Multiplex Fun Cub model." Mutiplex Modellsport GmbH & Co. KG. [Online]. Available: https://shop.multiplex-rc.de/en/rr-funcub-ng-blue-p4212/ (Accessed: Aug. 05, 2024).

[27] "XFLR5 – Browse Files at SourceForge.net." SourceForge. [Online]. Available: https://sourceforge.net/projects/xflr5/files/ (Accessed: Aug. 04, 2024).

[28] A. Septiyana *et al.*, "Analysis of aerodynamic characteristics using the vortex lattice method on twin tail boom unmanned aircraft," in *3rd International Seminar on Metallurgy and Materials (ISMM2019): Exploring New Innovation in Metallurgy and Materials, Tangerang Selatan*, Indonesia, 2020, p. 020003, doi: 10.1063/5.0002337.

[29] B.M. Simmons, "System Identification of a Nonlinear Flight Dynamics Model for a Small, Fixed-Wing UAV," Virginia Tech., 2018. [Online]. Available: http://hdl.handle.net/10919/95324 (Accessed: Aug. 04, 2024).

[30] C. Deiler, "Aerodynamic Modeling, System Identification, and Analysis of Iced Aircraft Configurations," *J. Aircr.*, vol. 55, no. 1, pp. 145–161, Jan. 2018, doi: 10.2514/1.C034390.

[31] C. Seren, F. Bommier, L. Verdier, A. Bucharles, and D. Alazard, "Optimal Experiment and Input Design for Flight Test Protocol Optimization," in *AIAA Atmospheric Flight Mechanics Conference and Exhibit*, Keystone, Colorado, Aug. 2006, doi: 10.2514/6.2006-6280.

[32] P. Lichota, "Multi-Axis Inputs for Identification of a Reconfigurable Fixed-Wing UAV," *Aerospace*, vol. 7, no. 8, p. 113, Aug. 2020, doi: 10.3390/aerospace7080113.

[33] M.S. Roeser and N. Fezans, "Method for designing multi-input system identification signals using a compact time-frequency representation," *CEAS Aeronaut. J.*, vol. 12, no. 2, pp. 291–306, Apr. 2021, doi: 10.1007/s13272-021-00499-6.

[34] N. Fezans, C. Deiler, and M.S. Roeser, "Generation of a Dataset for System Identification with VIRTTAC-Castor," in *DLRK 2019*, 2019, [Online]. Available: https://elib.dlr.de/129105/ (Accessed: Aug. 04, 2024).

[35] M. Marchand, "Untersuchung der Bestimmbarkeit der flugmechanischen Derivative des CCV-Versuchsträgers F-104 G," Tech. Rep. DLR-IB 154-74/32, DLR Institute of Flight Mechanics, Brunswick, Germany, 1977.

[36] R. Koehler and K. Wilhelm, "Auslegung von Eingangssignalen für die Kennwertermittlung," Report IB 154–77/40, DFVLR Institut für Flugmechanik, Braunschweig, F.R. Germany, 1977, pp. 154–77.

[37] T.F.K. Cordeiro, J.P. L.C. Da Costa, K. Liu, and G.A. Borges, "Kalman-based attitude estimation for an UAV via an antenna array," in *2014 8th International Conference on Signal Processing and Communication Systems (ICSPCS)*, Gold Coast, Australia, Dec. 2014, pp. 1–10, doi: 10.1109/ICSPCS.2014.7021136.

[38] A. Symington, R. De Nardi, S. Julier, and S. Hailes, "Simulating quadrotor UAVs in outdoor scenarios," in *2014 IEEE/RSJ International Conference on Intelligent Robots and Systems*, Chicago, IL, USA, Sep. 2014, pp. 3382–3388, doi: 10.1109/IROS.2014.6943033.

[39] R.S. Stanković and B.J. Falkowski, "The Haar wavelet transform: its status and achievements," *Comput. Electr. Eng.*, vol. 29, no. 1, pp. 25–44, Jan. 2003, doi: 10.1016/S0045-7906(01)00011-8.

[40] E. Marciniak, M. Stopa, T. Marciniak, A. Stankiewicz, P. Rakowicz, and A. Dąbrowski, "Denoising methods for improving automatic segmentation in OCT images of human eye," *Bull. Pol. Acad. Sci. Tech. Sci.*, vol. 65, no. 1, pp. 71–78, 2017, doi: 10.1515/bpasts-2017-0009.

[41] C.M. Akujuobi, *Wavelets and Wavelet Transform Systems and Their Applications: A Digital Signal Processing Approach*. Cham: Springer International Publishing, 2022. doi: 10.1007/978-3-030-87528-2.

[42] L.P.A. Arts and E.L. van den Broek, "The fast continuous wavelet transformation (fCWT) for real-time, high-quality, noise-resistant time–frequency analysis," *Nat. Comput. Sci.*, vol. 2, no. 1, pp. 47–58, 2022, doi: 10.1038/s43588-021-00183-z.